

The Dynamics of Collapsing Monopoles and Regular Black Holes

Hyunji Cho, David Kastor and Jennie Traschen

*Department of Physics and Astronomy
University of Massachusetts
Amherst, MA 01003-4525 USA*

Abstract

We study the formation and stability of regular black holes by employing a thin shell approximation to the dynamics of collapsing magnetic monopoles. The core deSitter region of the monopole is matched across the shell to a Reissner-Nordstrom exterior. We find static configurations which are nonsingular black holes and also oscillatory trajectories about these static points that share the same causal structure. In these spacetimes the shell is always hidden behind the black hole horizon. We also find shell trajectories that pass through the asymptotically flat region and model collapse of a monopole to form a regular black hole. In addition there are trajectories in which the deSitter core encompasses a deSitter horizon and hence undergoes topological inflation. However, these always yield singular black holes and never have the shell passing through the asymptotically flat region. Although the regular black hole spacetimes satisfy the strong energy condition, they avoid the singularity theorems by failing to satisfy the genericity condition on the Riemann tensor. The regular black holes undergo a change in spatial topology in accordance with a theorem of Börde's.

February, 2000

1. Introduction

The purpose of this paper is to investigate the formation and stability of regular black holes. In 1968 Bardeen [1] presented an example of a black hole spacetime that satisfies the weak energy condition, contains a region of trapped surfaces, and yet has no curvature singularities. Recently Borde [2] proved a theorem that helps to clarify when regular black holes can occur. Borde showed that if a black hole spacetime contains trapped surfaces, satisfies the weak energy condition and is non-singular, then there must be a change of topology in the spacetime. Inside the horizon there is a region where the topology changes from open to compact spatial slices. The false-vacuum cores of topological defects typically satisfy the weak energy condition and have internal geometry that is approximately described by deSitter spacetime. Further, static magnetic monopole black hole spacetimes have been found in which the horizon is embedded in the monopole fields [3], rather than being completely collapsed into the singularity [4][5]. Therefore, monopole spacetimes are good candidates for examples of regular black holes, illustrating Borde's theorem in a physically interesting context.

We have found two further illustrative examples of regular black holes in the literature, though neither was commented on as such by the authors. Boulware's paper on dynamical charged dust shells [6] contains a spacetime diagram of a charged shell which collapses to form a regular $Q = M$ extremal black hole. The singularity is completely covered by the Minkowski interior of the shell. Tachizawa et. al. [7] display three spacetime diagrams, reproduced in figures (1a,c,d) below that follow from approximate solution for a static, gravitating monopole [3]. In these figures the exterior, unshaded region of the spacetime is magnetically charged Reissner-Nordstrom (RN) and the interior, shaded region is deSitter (dS), which approximates the monopole core. Depending on the values for the magnetic charge and the cosmological constant, these spacetimes have either (a) $Q > M$ and no horizons, (c) $Q < M$ with black hole horizons, but no deSitter horizon, or (d) $Q < M$ with black hole and deSitter horizons. There is also an extremal $Q = M$ case shown in figure (1b). The three black hole spacetimes are regular. The spatial slices S_1 and S_2 show the transition from open $S^2 \times R$ to compact S^3 spatial sections.

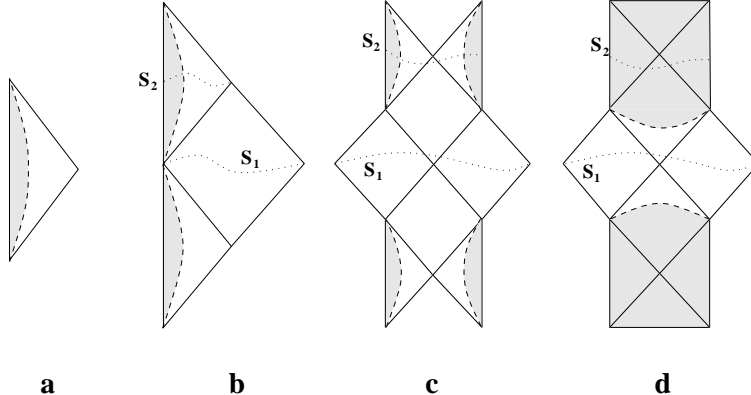


Figure. 1: Static monopole shell configurations. The dashed lines denote the static monopole shell. The unshaded regions are Reissner-Nordstrom. The shaded regions are deSitter. The corresponding ranges of the dimensionless parameter η are (a) $\eta < 3/2$, (b) $\eta = 3/2$, (c) $3/2 < \eta\sqrt{3}$ and (d) $\sqrt{3} < \eta$.

We would like to study the formation of such regular black holes via collapse. The dynamics of the full Einstein-YM-Higgs system has been studied numerically in [8]. In order to obtain analytic results, here we will make use of a thin shell approximation for the monopole instead. The system will be described by the false vacuum energy density, or cosmological constant Λ , the mass M of the spacetime, the charge Q and the mass per unit area σ of the shell¹. Clearly one loses the detailed non-abelian structure monopole in this model. At the end of the introduction we will argue that the shell approximation is qualitatively correct when the energy density of the monopole core is dominated by the false vacuum energy.

Before adding shells of stress energy, consider the following static, spherically symmetric model of a gravitating monopole [3][7],

$$ds^2 = -A(r)dt^2 + \frac{dr^2}{A(r)} + r^2d\Omega^2. \quad (1)$$

The core energy density is dominated by the vacuum potential energy, and far from the core the energy density goes to zero like r^{-4} . The spacetime should interpolate between a

¹ After this work was completed, references [9] and [10] appeared which also study the dynamics of magnetic monopoles using the thin shell approximation employed here. These papers include many of the same results, although with somewhat different emphasis in the analysis. In particular, reference [9] includes the possibility of a cosmological constant in the region exterior to the monopole and uses the AdS/CFT correspondence to address the uniqueness of evolution of the shell trajectory through Cauchy horizons. Reference [10] gives a complete analysis of possible trajectories for the monopole shell in terms of the mass M and charge Q of the spacetime and the ratio k of the interior false vacuum energy density to the surface energy density of the shell.

core deSitter region and a magnetically charged Reissner-Nordstrom exterior. In fact, the two regions can be matched directly across a charged shell at radius R giving

$$\begin{aligned} A(r) &= A_{dS}(r) = 1 - H^2 r^2, \quad r < R \\ A(r) &= A_{RN}(r) = 1 - \frac{2M}{r} + \frac{Q^2}{r^2}, \quad r > R \end{aligned} \quad (2)$$

Requiring that the metric and its first derivative be continuous fixes the matching radius R and the ADM mass M in terms of the charge Q and the cosmological constant $\Lambda = 3H^2$,

$$\frac{R}{Q} = \frac{1}{\eta}, \quad \frac{M}{Q} = \frac{2}{3}\eta, \quad \eta^2 = \sqrt{3}QH. \quad (3)$$

References [3][7] discuss the metric (2) as an approximation to their more detailed numerical results. We want to stress here that the metric (2) subject to (3) is actually a solution to the Einstein-Maxwell equations. There is *no* shell of stress energy at the matching radius, but there is a shell of charge. Further it is interesting to note that if one wants to match Minkowski to Schwarzschild [11], Minkowski to RN [6], or deSitter to Schwarzschild [12], a shell of stress energy is needed to do the matching. A deSitter interior can also be matched directly to flat space minus a solid angle, the asymptotic exterior of a global monopole with no shell of stress energy. Reference [13] then further adds a shell to study the dynamics of this model of a global monopole.

The resulting spacetime diagrams from the matching are then those of figure (1), with the different cases corresponding to different ranges of the dimensionless variable η . For $0 < \eta < 3/2$ we have $Q > M$ and there are no horizons in the spacetime as in figure (1a). Therefore, this can be considered a weakly gravitating monopole. For $\eta = 3/2$ we have $Q = M$ as in figure (1b). For $3/2 < \eta < \sqrt{3}$ we have $Q < M$ with the matching radius R such that both black hole horizons are present outside the shell, but no deSitter horizon inside. For $\sqrt{3} < \eta$ we have $Q < M$ with only the outer black hole horizon present outside the matching radius. In this case the inner deSitter region extends through a cosmological horizon as well. Note that in this case the boundary between regions is a spacelike surface, and therefore is more like a phase transition in the spacetime. We will not be considering spacetimes of this type in the present work.

When one adds a shell of stress energy at the matching radius, the spacetime becomes dynamical. The shell generically collapses, expands, or oscillates. The spacetimes described by (2) are robust in the sense that there continue to be static shell solutions, and also solutions in which the shell oscillates about the static points. In these cases the black

holes are regular, since the shell radius is bounded away from zero and inside the shell the spacetime is always deSitter. There are regular extremal and non-extremal black holes of this type. In the extended RN spacetime there is a sequence of repeating timelike singularities as one moves up the diagram. In order for the extended spacetime to be regular, one would need to cover each singularity with a shell. From the asymptotically flat region these black holes look just like any RN black hole.

A second type of dynamical solution describes a monopole that collapses to form a black hole. These are shells that pass through the asymptotically flat region for some portion of the trajectory. One can imagine starting the evolution of a monopole as the shell passes through this region and watching it collapse inside its horizon. It turns out that all shells that pass through the asymptotically flat region correspond to shell oscillations around a local minimum of an effective potential. In the extended spacetimes, these oscillations take the shell repeatedly out through white hole horizons and back into black hole horizons. Since the shell radius is bounded, the interior of the shell is regular. In particular, in the extremal case a single oscillating shell, which passes through the asymptotically flat region, covers up all the singularities of the RN spacetime, giving a maximally extended regular black hole spacetime. In the non-extremal case, however, there are RN singularities on both sides of the diagram, only one set of which is covered up by a single oscillating shell trajectory. One would have to add additional shells to cover up the singularity on the other side of the spacetime.

The possibility of topological inflation has been studied in the literature [14][15]. This refers to the case when the core of a topological defect is approximately described by a deSitter metric and includes a deSitter, or cosmological, horizon. There are many shell trajectories in the present case which contain inflating cores. All of these are singular black holes, and the shell never passes through the asymptotically flat region in any of the inflating cases. So this is a kind of null result. In this stripped down model, an observer in the asymptotically flat region would never see a monopole collapse which is bound to evolve into an inflating cosmology.

How do the regular black hole spacetimes we find in this paper, as well as the earlier Bardeen example, avoid forming singularities? Penrose's (1965) singularity theorem [16] requires that the spacetime be globally hyperbolic, and the later (1970) singularity theorem of Hawking and Penrose [17] requires instead a genericity condition on the Riemann tensor. None of these examples are generic, or globally hyperbolic. The regular $Q < M$ examples illustrate the spatial topology change required by Börde's theorem. He discusses how,

although light rays are focused in the region of trapped surfaces, the change to the three-sphere topology allows focusing without the formation of a singularity. The extremal, $Q = M$ spacetimes do not contain trapped surfaces and therefore do not fall within the scope of Börde's theorem. Nonetheless, the spatial topology changes inside the horizon.

We conclude the introduction with a simple comparison of the shell model for gravitating monopoles to features of nongravitating monopoles. Compare the relations (3), which give the mass and core radius of the static gravitating monopole spacetime in terms of the charge and vacuum energy density, to analogous relations for non-gravitating monopoles. An 't Hooft-Polyakov monopole is described by three parameters; the Higgs vacuum expectation value v , its self-coupling λ and the gauge coupling constant e (see *e.g.* [18]). The monopole then has charge $Q \sim 1/e$, mass $M \sim v/e$ and core radius $R \sim 1/(ev)$. This implies an average energy density of the core $\rho \sim e^2 v^4$. Now, define a 'Hubble constant' for the monopole by $H^2 \sim \rho \sim e^2 v^4$. Trading the parameters Q, H for v, e gives $M \sim (Q^3 H)^{1/2}$ and $R \sim \left(\frac{Q}{H}\right)^{1/2}$, which have the same functional dependence on Q, H as in (3).

Where did the parameter λ go to? For the core to be dominated by the vacuum energy density, and hence for the metric in the core region to be well approximated by deSitter, one would expect $H^2 \sim V_{false} \sim \lambda v^4$. In order that this expression for H agree with our previous estimate in the monopole core, we need that $e^2 \sim \lambda$. So for such monopoles, we have this qualitative motivation that the simple gravitational model (1), (2), (3) is a model of a monopole.

2. Collapsing Magnetic Monopoles

We model a collapsing magnetic monopole by a charged, spherically symmetric domain wall, or shell, that separates a region of deSitter spacetime inside the shell from a region of Reissner-Nordstrom spacetime outside. The domain wall has constant surface energy density σ , total magnetic charge Q and time dependent radius $R(\tau)$, where τ is the proper time for a worldline with constant angular position on the domain wall. The spacetime metric then has the form (1) with

$$A(r) = \begin{cases} A_{dS}(r), & r < R(\tau) \\ A_{RN}(r), & r > R(\tau) \end{cases} \quad (4)$$

By Gauss's law the total charge Q of the shell must be the same as the charge Q appearing in the exterior RN metric function (2).

Shell Dynamics

The dynamics of the shell are determined using the Israel shell formalism [19], which imposes Einstein's equation including the distributional stress-energy of the shell. In the present case, there are also contributions to T_{ab} from the cosmological constant inside the shell and the Maxwell stress-energy outside. The motion of the shell is described by its four-velocity, which we take to be radially directed, $u^a = u^t \frac{\partial}{\partial t} + u^r \frac{\partial}{\partial r}$, and normalized, $u^a u_a = -1$. The unit normal to the shell is also radially directed, and satisfies $n^a u_a = 0$, $n^a n_a = +1$. In general the stress-energy of a spherically symmetric shell is described by two parameters, the mass per unit area σ and the pressure p . Israel's shell formalism relates the jump in the extrinsic curvature K_{ab} of the shell to integrals of the shell stress-energy. The jump in $K_{\tau\tau}$ gives the evolution equation for σ , $\dot{\sigma} = -2 \frac{\dot{R}}{R}(\sigma - p)$. Dust shells have zero pressure, and so $\sigma \sim R^{-2}$ which implies that the total mass of the shell is constant. Domain walls have $\sigma = p$ and so σ is constant. In this work we model the monopole shell as a domain wall.

The other jump condition can be summarized simply in terms of the jump in the radial components of the outward pointing unit normal vectors to the shell, n_{dS}^r and n_{RN}^r , which are evaluated just inside and just outside the shell respectively,

$$r[K_\theta^{\theta}]_{RN}^{dS} = n_{dS}^r - n_{RN}^r = 4\pi\sigma R(\tau). \quad (5)$$

For $Q = 0$ this reduces to the case studied in [12]. This condition determines the motion of the shell as follows. The squares of the radial normal components satisfy

$$(n_{dS}^r)^2 = A_{dS}(R) + \dot{R}^2, \quad (n_{RN}^r)^2 = A_{RN}(R) + \dot{R}^2, \quad (6)$$

where $\dot{R} = dR/d\tau$. Squaring equation (5) and substituting in (6) yields the relations

$$n_{RN}^r = \frac{1}{8\pi\sigma R}(A_{dS} - A_{RN} - 16\pi^2\sigma^2 R^2), \quad n_{dS}^r = \frac{1}{8\pi\sigma R}(A_{dS} - A_{RN} + 16\pi^2\sigma^2 R^2) \quad (7)$$

Squaring these equations and using (6) again then gives the alternate forms

$$\begin{aligned} \dot{R}^2 &= \frac{1}{(8\pi\sigma R)^2}(A_{dS} - A_{RN} - 16\pi^2\sigma^2 R^2)^2 - A_{RN} \\ \dot{R}^2 &= \frac{1}{(8\pi\sigma R)^2}(A_{dS} - A_{RN} + 16\pi^2\sigma^2 R^2)^2 - A_{dS} \end{aligned} \quad (8)$$

Following reference [12], we introduce rescaled dimensionless coordinates and variables. The rescaled radial coordinate of the shell $z(\tau')$ is regarded as a function of the rescaled time parameter τ' with

$$z = \left(\frac{H^2 + 16\pi^2\sigma^2}{2M} \right)^{1/3} R, \quad \tau' = \left(\frac{H^2 + 16\pi^2\sigma^2}{8\pi\sigma} \right) \tau \quad (9)$$

We then rewrite equation (8) in the form of particle motion in an effective potential $V(z)$.

$$\left(\frac{dz}{d\tau'} \right)^2 + V(z) = E \quad (10)$$

with the potential given in terms of dimensionless parameters α, γ by

$$V(z) = -\frac{1}{z^2} \left(z^2 - \frac{1}{z} + \frac{\alpha}{z^2} \right)^2 - \gamma^2 \left(\frac{1}{z} - \frac{\alpha}{z^2} \right). \quad (11)$$

The energy E and the parameters α, γ are given by

$$E = -\frac{64\pi^2\sigma^2}{(2Mh^2)^{2/3}}, \quad \alpha = \frac{Q^2h^{2/3}}{(2M)^{4/3}}, \quad \gamma = \frac{8\pi\sigma}{h}, \quad (12)$$

where $h^2 = H^2 + 16\pi^2\sigma^2$. Note that γ varies only over the range $0 \leq \gamma \leq 2$. The problem began with four dimensional parameters H, M, Q and σ . Through the rescaling, this has been reduced to the three dimensionless parameters α, γ and E .

Shape of the Potential

One now analyzes the different types shell motion by studying the possible shapes for the potential depending on the parameters α and γ and then considering different values of the energy E for a fixed potential. The potential $V(z) \rightarrow -\infty$ both as $z \rightarrow 0$ and as $z \rightarrow \infty$. In between, the potential may, or may not, have a local minimum depending on α, γ (see figures (2a) and (2b)). For $\alpha = 0$, which gives the $Q = 0$ case studied in [12], there is never a local minimum. The repulsive Coulomb self-interaction of the $\alpha > 0$ shell is therefore responsible for the possibility of stable static configurations as in figure (2b). Such local minima are also present in the analysis of global monopoles in [13].

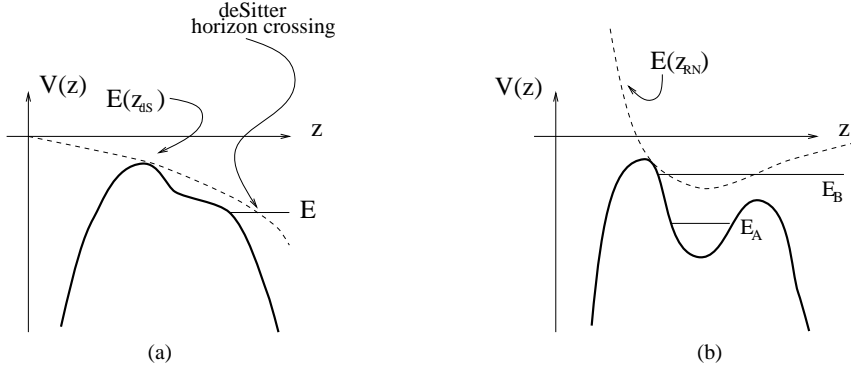


Figure. 2: The potential $V(z)$ can either (a) have no local minimum, or (b) have a local minimum, depending on the values of the parameters α and γ . In (2a) we have sketched in the deSitter horizon curve $E(z_{dS})$ and shown a shell trajectory that crosses the horizon. Figure (2b) includes the Reissner-Nordstrom horizon curve and trajectories with energies E_A that falls below this curve and hence has $Q > M$ and E_B that has $Q < M$ and crosses both inner and outer RN horizons.

In detail, we find that the potential $V(z)$ always has a local minimum if $0 < \alpha < \alpha_1$, with $\alpha_1 = (\frac{1}{2})^{4/3}$. For α in the range $\alpha_1 < \alpha < \alpha_2$, with $\alpha_2 = \frac{3}{4^{4/3}}$, there exists a value γ_{max}^2 that depends on α , such that $V(z)$ has a local minimum only for $\gamma^2 < \gamma_{max}^2$. If $\alpha_2 < \alpha$, then $V(z)$ does not have a local minimum for any value of γ .

Horizon Curves

Given fixed values for the parameters H , M , Q and σ , the deSitter and Reissner-Nordstrom metrics respectively have horizons at

$$r_{dS} = \frac{1}{H}, \quad r_{RN}^\pm = M \pm \sqrt{M^2 - Q^2}. \quad (13)$$

The corresponding dimensionless coordinates for the horizons,

$$z_{dS} = \frac{2\sqrt{|E|}}{\gamma(4 - \gamma^2)^{1/2}}, \quad z_{RN}^\pm = \frac{\gamma^2 \pm \sqrt{\gamma^4 - 4|E|\alpha\gamma^2}}{2|E|} \quad (14)$$

are then functions of the parameters α and γ that determine the shape of the potential and also of the particle energy E . Whether, or not, a shell trajectory crosses through the various horizon radii determines the causal structure of the resulting spacetime. Since the horizon radii expressed in terms of the dimensionless radial variable z are energy dependent, it is useful to plot horizon curves on the potential diagrams as well. In order to do this, we invert the relationships (14) to get the energies E_{dS} and E_{RN} that correspond to given values of the horizon radii

$$E_{dS}(z_{dS}) = -\gamma^2 \left(1 - \frac{\gamma^2}{4}\right) z_{dS}^2, \quad E_{RN}(z_{RN}) = -\gamma^2 \left(\frac{1}{z_{RN}} - \frac{\alpha}{(z_{RN})^2}\right) \quad (15)$$

A shell trajectory then passes through a given horizon if its constant energy line on the potential diagram intersects the corresponding horizon curve. For example, in figure (2a) we have sketched in both the deSitter horizon curve and the trajectory of a shell that passes through the deSitter horizon.

From equation (14) we can see that in terms of the dimensionless variables, horizons exist only for $4\alpha|E| \leq \gamma^2$, with $4\alpha|E| = \gamma^2$ being the extremal $Q = M$ limit. The Reissner-Nordstrom horizon curve has the limit $E_{RN}(z) \rightarrow \infty$ for $z \rightarrow 0$ and approaches zero from below as $z \rightarrow \infty$. In between it has a minimum at $E_{ext} = -\gamma^2/4\alpha$. Shell trajectories with $E > E_{ext}$ correspond to $Q < M$ spacetimes, trajectories with $E = E_{ext}$ have $Q = M$ and trajectories with $E < E_{ext}$ have $Q > M$.

Signs of the radial normals

One can see from equation (7) that the radial normals n_{dS}^r and n_{RN}^r can have either sign and that in particular $n_{RN}^r < 0$ for sufficiently large, or small, shell radius R . By definition the normal vectors point away from the deSitter region and into the Reissner-Nordstrom region. The sign of n_{RN}^r determines whether, in moving into the Reissner-Nordstrom region the radial coordinate is increasing, or decreasing.

The actual signs of n_{dS}^r and n_{RN}^r are very useful in analyzing the motion. We can see that the points where these quantities pass through zero are given by the places where the horizon curves $E_{dS}(z)$ and $E_{RN}(z)$ intersect the potential $V(z)$. First rewrite the expressions (7) for n_{dS}^r and n_{RN}^r in terms of dimensionless quantities

$$n_{dS}^r = \frac{-\left(1 - \frac{\gamma^2}{2}\right)z^4 + z - \alpha}{z^3\sqrt{-E}}, \quad n_{RN}^r = \frac{-z^4 + z - \alpha}{z^3\sqrt{-E}} \quad (16)$$

Now rewrite the horizon curves $E_{dS}(z)$ and $E_{RN}(z)$ separating out explicitly a factor of the potential $V(z)$

$$\begin{aligned} E_{dS}(z) &= V(z) + \left\{ \frac{1}{z^3} \left[-\left(\frac{1 - \gamma^2}{2} \right) z^4 + z - \alpha \right] \right\}^2 \\ E_{RN}(z) &= V(z) + \left[\frac{-z^4 + z - \alpha}{z^3} \right]^2 \end{aligned} \quad (17)$$

We see that the radial normals n_{dS}^r and n_{RN}^r vanish precisely when the horizon curves the potential meet.

The radial normals will have zeroes only for over certain ranges of the parameters α and γ . In detail we find that for $\alpha < \alpha_2$, the potential $V(z)$ and the Reissner-Nordström

horizon line meet at two radii, z_{RN-} and z_{RN+} . Within the range $z_{RN-} < z < z_{RN+}$, the radial normal $n_{RN}^r > 0$, while for $z < z_{RN-}$ and $z > z_{RN+}$ the radial normal $n_{RN}^r < 0$. For $\alpha > \alpha_2$, the horizon line is always above the potential and n_{RN}^r is always negative.

For the sign of the radial normal n_{dS}^r we find that for $\gamma^2 \geq 2$, the potential and the De Sitter horizon curve meet each other at a single radius z_{dS} . The radial normal satisfies $n_{dS}^r < 0$ for $z < z_{dS}$ and $n_{dS}^r \geq 0$ for $z \geq z_{dS}$ independent of the value of α . For $\gamma^2 < 2$, the sign on n_{dS}^r depends on α . For $\alpha < \alpha_2$ and $\gamma < 2$, the potential and the deSitter horizon curve meet at two points, which we label z_{dS-} and z_{dS+} . For $z_{dS-} \leq z \leq z_{dS+}$, we have $n_{dS}^r \geq 0$, with $n_{dS}^r \leq 0$ otherwise. When $\alpha_2 < \alpha$ and $2\left(1 - \frac{\alpha_2^3}{\alpha^3}\right) < \gamma^2 < 2$, the result is the same. However, for $\gamma^2 < 2\left(1 - \frac{\alpha_2^3}{\alpha^3}\right)$, $n_{dS}^r < 0$ always holds..

3. Summary of Results

Clearly, there are many possible trajectories for the shells. In this section we will give a summary of the different types of motion and the resulting causal structures. Our primary interest is in whether, or not, there are shell trajectories in which the monopole collapses to form a regular black hole. A full tabulation of different types of shell motions is given in appendix A. In particular, table (1) in appendix A lists the different possible types of shell motion viewed from the Reissner-Nordstrom side of the spacetime. In figures (10)-(16) examples of these trajectories are shown on potential diagrams that include the RN horizon line and the points $z_{RN\pm}$ where the radial normal n_{dS}^r changes sign. Table (2) and figures (17)-(19) give similar information with respect to the deSitter portion of the spacetime. Finally, table (3) relates the forms of potentials and horizon lines in figures (10)-(19) to specific ranges of the parameters α and γ . It may be helpful for the reader to refer to these figures while reading through the present section.

In the figure below, we reproduce figure (2b) with different shell energies drawn in for reference. For each of these levels there will be examples with $Q < M$, $Q = M$ and $Q > M$, depending on whether the energy level lies above or below the RN horizon curve. In addition for $Q \leq M$ whether, or not, a shell trajectory crosses the RN horizon line will lead to distinct causal structures. Since our primary interest is in shell trajectories that lead to regular black holes, the important feature of the deSitter interior of the shell for us is its regularity. However, we will also note for each class of trajectories whether the shell passes through a deSitter horizon and hence undergoes topological inflation in its interior.

- *Type 0:* These are static shell configurations, generalizations of the static $\sigma = 0$ solutions presented in the introduction for the timelike boundaries and shown in figures (1a-1c)².

² Recall the matching in figure (1d) is along a spacelike shell.

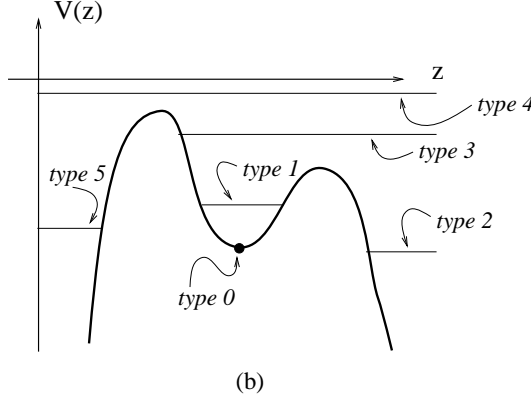


Figure. 3: Sketch of a potential diagrams showing shell energy levels of different basic types.

The Penrose diagrams are again those of figures (1a-c). Note that each shell covers only one singularity. For the maximally extended regular black holes shown in the figures, we need a separate shell covering each of the singularities. Also note that from figure (17) we can confirm that the shell radius is always smaller than the deSitter horizon radius for the static configurations. Hence the shell interior does not include an inflating region.

- *Type 1:* In type I trajectories the shell oscillates between minimum and maximum radii. For $Q < M$, $Q = M$ and $Q > M$ there are three configurations, trajectories (d), (f) and (h) in table (1), that have Penrose diagrams resembling those for the static (*i.e.* type 0) solutions but with an infinite number of oscillations in the shell trajectory as it goes from past to future timelike infinity. The existence of these trajectories demonstrates the stability of the static monopole shells to small oscillations. In addition, for $Q < M$ and $Q = M$, there are oscillatory trajectories shown in figure (4) that repeatedly pass out through white hole horizons and in through black hole horizons as they traverse the fully extended spacetime. These are trajectories (e) and (g) in table (1). These shells pass through region I at some time. If we pick a spacelike surface in region I as an initial data surface, then an observer in region I sees a monopole collapsing to form a black hole. The $Q = M$ case illustrates collapse of a single shell to form a regular black hole. Note that in order to figure out which of the singularities in the $Q = M$ diagram is covered up by the shell, we use the fact that the normal n_{RN}^r is positive everywhere along the path. In region II^+ the normal is positive, *i.e.* moving into the Reissner-Nordstrom region is moving to larger values of the radial coordinate, while in region II^- it is negative. Finally, like the static configurations the shell radius is always smaller than the deSitter horizon radius for the type 1 trajectories. Hence our regular black hole solutions do not include inflating cores.

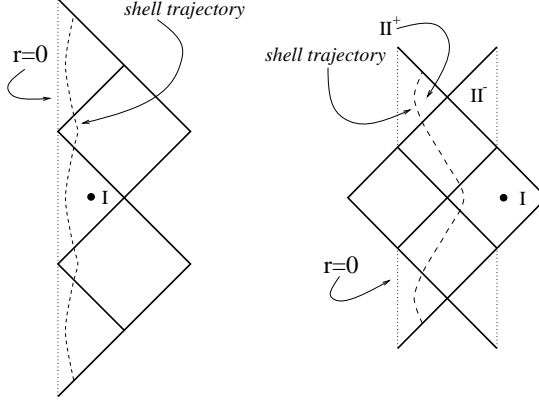


Figure. 4: Type 1 trajectories. Here and below, the solid dot denotes the Reissner-Norstrom side of the shell. The opposite side of the spacetime diagram is replaced with the deSitter interior of the shell. The $Q = M$ example shows collapse of a single shell to form a regular black hole. The $Q < M$ case would need additional shells to cover up all singularities in future of region I.

- *Type 2:* Trajectories of types 2, 3 and 4 all start from $R = \infty$. Note that equation (7) implies that for large shell radii the sign of the normal n_{RN}^r is always negative. The normal vector by definition points away from the deSitter region into the Reissner-Nordstrom region. The sign of the radial component being negative implies that moving from the shell into the RN part of the spacetime, the radial coordinate is decreasing³. If we have $n_{RN}^r < 0$ in an asymptotically flat part of the spacetime, this indicates that the shell is on the left hand side of the Penrose diagram.

For type 2 trajectories, there is one type of shell path for $Q > M$ and two types each for $Q = M$ and $Q < M$. One set of possibilities for $Q > M$, $Q = M$ and $Q < M$ respectively is given by trajectories (i), (j) and (m) in table (1), which are shown in figure (10). These trajectories have no horizon crossings and always remain in a region with $n_{RN}^r < 0$. The RN portions of the spacetime diagrams are shown in figure (5). We see from figure (5) that the $Q \geq M$ spacetimes have no asymptotically flat region. The $Q < M$ spacetimes contains the asymptotically flat region on the left hand side of the diagram. However, the monopole shell never passes through this region and these spacetimes are still singular. From the point of view of the deSitter interior, we can see from *e.g.* figure (17) that trajectories of type 2 always start outside the deSitter horizon, pass in through the horizon and then cross out again.

³ Although this appears contrary to equation, in fact the results continue to hold.

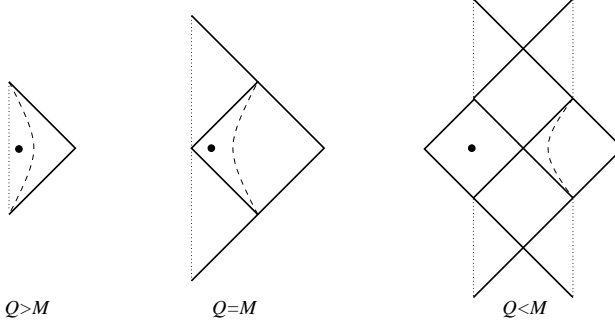


Figure. 5: Type 2 trajectories (i), (j) and (m) respectively. In each case the RN region is to the left of the shell trajectory since $n_{RN}^r < 0$.

The second set of possibilities for $Q = M$ and $Q < M$, trajectories (k) and (n) in table (1), cross horizons but still have $n_{RN}^r < 0$ everywhere along the path. These are shown in figure (6). Again we see that the $Q = M$ spacetimes have no asymptotically flat region and that in the $Q < M$ spacetimes the monopole shell is never passes through the asymptotically flat region.

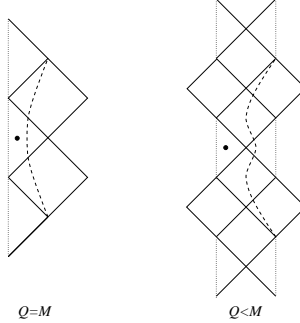


Figure. 6: Type 2 trajectories (k) and (n). In each case the RN region is to the left of the shell trajectory.

- *Type 3:* There are one $Q = M$ trajectory and two $Q < M$ trajectories, (l), (o) and (p) in table (1) respectively. Trajectories (l) and (o) have the form shown in figure (6) above, while trajectory (p) has the form shown in figure (7). The qualitative differences between trajectories (o) and (p) involve only how the sign of the normal changes along the curve. Again in the $Q < M$ spacetimes the shell is never passes through an asymptotically flat region of the spacetime. The type 3 trajectories viewed from the deSitter interior also always pass in and then out of the deSitter horizon.
- *Type 4:* These trajectories move in from infinity and hit the curvature singularity at $R = 0$ in finite proper time. There is one possibility for $Q > M$ - trajectory (q); one for $Q = M$ - trajectory (r); and two for $Q < M$ - trajectories (s) and (t), all shown in figure (8). The Reissner-Nordstrom portions of these spacetimes are all singular and again are

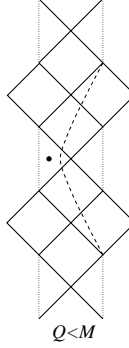


Figure. 7: Type 3 trajectory (p). Again the RN region is to the left of the curve.

uninteresting for our purposes. Again the $Q \geq M$ spacetimes are not asymptotically flat and the monopole shell does not pass through the asymptotically flat region of the $Q < M$ spacetimes. In these spacetimes the shell passes in through the deSitter horizon, but then never exits. Thus they include a past deSitter horizon, but not a future horizon.

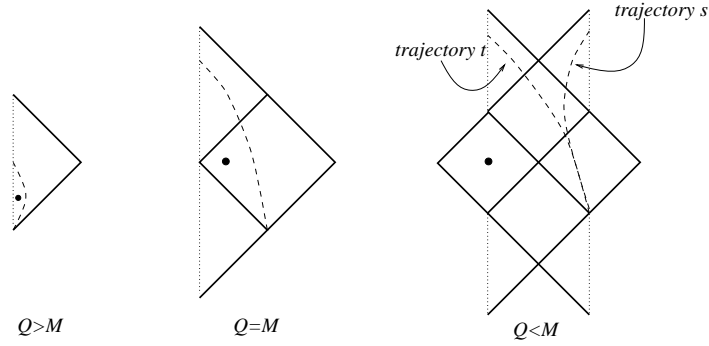


Figure. 8: Type 4 trajectories (q), (r), (s) and (t).

- *Type 5:* Finally, type 5 trajectories (a), (b) and (c) leave $R = 0$ and return within finite proper time. All of these spacetimes contain naked singularities. The Reissner-Nordstrom sides of the spacetime diagrams are shown in figure (9).

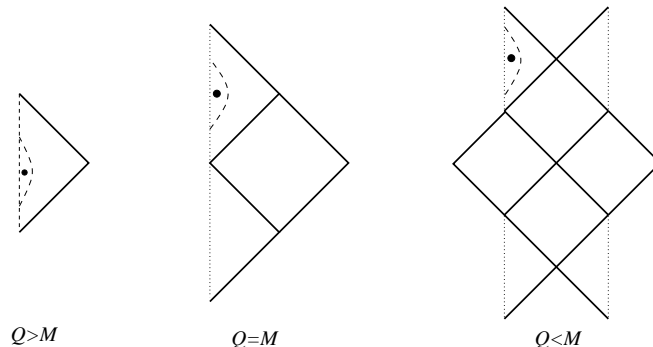


Figure. 9: Type 5 trajectories (a), (b) and (c) depart and return to the curvature singularity $R = 0$ in finite proper time.

Appendix A.

Table (1) summarizes the qualitatively different possible shell trajectories when viewed from the Reissner-Nordstrom part of the spacetime. The various paths (st1, st2, st3) and (a-t) are labeled on the potential diagrams in figures (9-16).

path	range of z	Sign of n_{RN}^r	Q and M	Horizon Crossing
a	$0 < z \leq z_{max}$	—	$Q > M$	*
b	$0 < z \leq z_{max}$	—	$Q = M$	no
c	$0 < z \leq z_{max}$	—	$Q < M$	no
st1	$z = z_{st}$	+	$Q > M$	*
st2	$z = z_{st}$	+	$Q = M$	no
st3	$z = z_{st}$	+	$Q < M$	no
d	$z_{min} \leq z \leq z_{max}$	+	$Q > M$	*
e	$z_{min} \leq z \leq z_{max}$	+	$Q = M$	yes
f	$z_{min} \leq z \leq z_{max}$	+	$Q = M$	no
g	$z_{min} \leq z \leq z_{max}$	+	$Q < M$	yes
h	$z_{min} \leq z \leq z_{max}$	+	$Q < M$	no
i	$z_{min} \leq z < \infty$	—	$Q > M$	*
j	$z_{min} \leq z < \infty$	—	$Q = M$	**
k	$z_{min} \leq z < \infty$	—	$Q = M$	yes
l	$z_{min} \leq z < \infty$	+-	$Q = M$	yes
m	$z_{min} \leq z < \infty$	—	$Q < M$	**
n	$z_{min} \leq z < \infty$	—	$Q < M$	yes
o	$z_{min} \leq z < \infty$	+-	$Q < M$	yes
p	$z_{min} \leq z < \infty$	- + -	$Q < M$	yes
q	$0 < z < \infty$	—	$Q > M$	*
r	$0 < z < \infty$	—	$Q = M$	yes
s	$0 < z < \infty$	- + -	$Q < M$	yes
t	$0 < z < \infty$	—	$Q < M$	yes

Table 1. Character of each path of the shell- Reissner-Nordström part

* $Q > M$ - no black hole horizons.

** There is no horizon present in the spacetime, since they (it) occur(s) inside the shell.

Table (2) summarizes the qualitatively different possible shell trajectories when viewed from the deSitter part of the spacetime. The various paths (ST) and (A-H) are labeled on the potential diagrams in figures (17-21).

Path	Range of z	Sign of n_{dS}^r	Horizon Crossing
A	$0 < z \leq z_{max}$	—	*
ST	$z = z_{st}$	+	*
B	$z_{min} \leq z \leq z_{max}$	+	*
C	$z_{min} \leq z < \infty$	+	yes
D	$z_{min} \leq z < \infty$	+-	yes
E	$z_{min} \leq z < \infty$	—	yes
F	$0 < z < \infty$	—	yes
G	$0 < z < \infty$	—+	yes
H	$0 < z < \infty$	—+—	yes

Table 2. Character of each path of the shell - de Sitter part

* The de Sitter horizon does not exist in these spacetimes since it lies outside the shell.

Table (3) lists the ranges of parameters α and γ that are relevant to the configurations of potentials and horizon curves shown in figures (10)-(19).

α	γ^2	$V - V_{dS}$	$V - V_{RN}$
$\alpha < \left(\frac{1}{2}\right)^{4/3}$	$\gamma^2 < 2$	I	1
	$\gamma^2 \geq 2$	II	1
$\left(\frac{1}{2}\right)^{4/3} < \alpha < \alpha_0$	$\gamma^2 < 2$	I	2,3,4
	$2 \leq \gamma^2 < \gamma_{max}^2$	II	2
	$\gamma^2 \geq \gamma_{max}^2$	III	5
$\alpha = \alpha_0$	$\gamma^2 < 2 (= \gamma_{max}^2)$	I	2,3,4
	$\gamma^2 \geq 2 (= \gamma_{max}^2)$	III	5
$\alpha_0 < \alpha < \frac{3}{4^{4/3}}$	$\gamma^2 < \gamma_{max}^2$	I	2,3,4
	$\gamma_{max}^2 \leq \gamma^2 < 2$	IV	5
	$\gamma^2 > 2$	III	5
$\alpha > \frac{3}{4^{4/3}}$	$\gamma^2 < 2 \left(1 - \frac{27}{256\alpha^3}\right)$	V	6,7,8
	$2 \left(1 - \frac{27}{256\alpha^3}\right) < \gamma^2 < 2$	IV	6,7,8
	$\gamma^2 \geq 2$	III	6,7,8

Table 3.

*For $\alpha = \alpha_0 (= 0.40418572)$, $\gamma_{max}^2 = 2$.

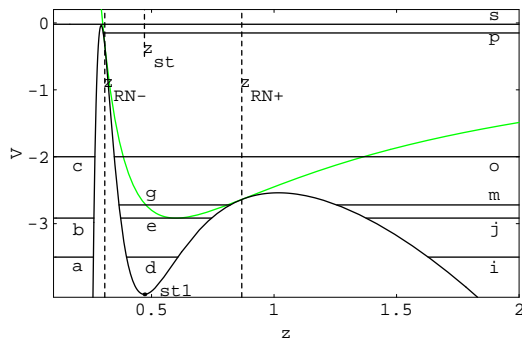


Figure. 10: Reissner-Nordstrom configuration 1.

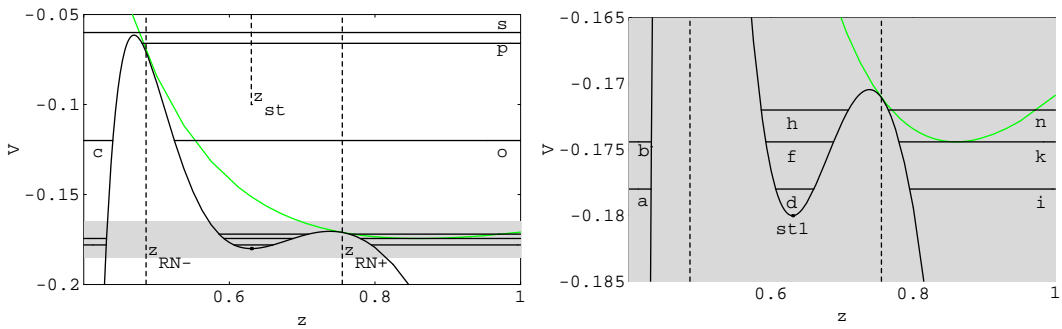


Figure. 11: Reissner-Nordstrom configuration 2.

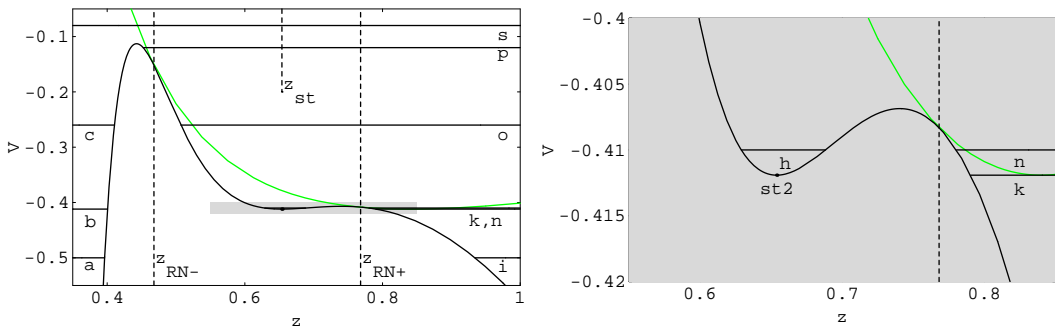


Figure. 12: Reissner-Nordstrom configuration 3.

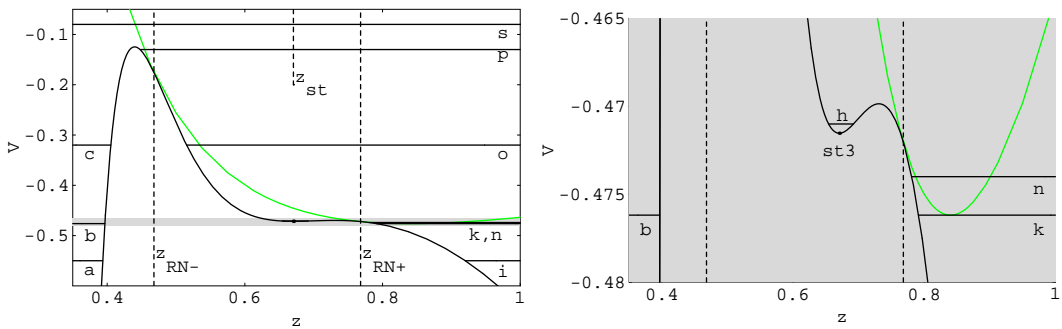


Figure. 13: Reissner-Nordstrom configuration 4.

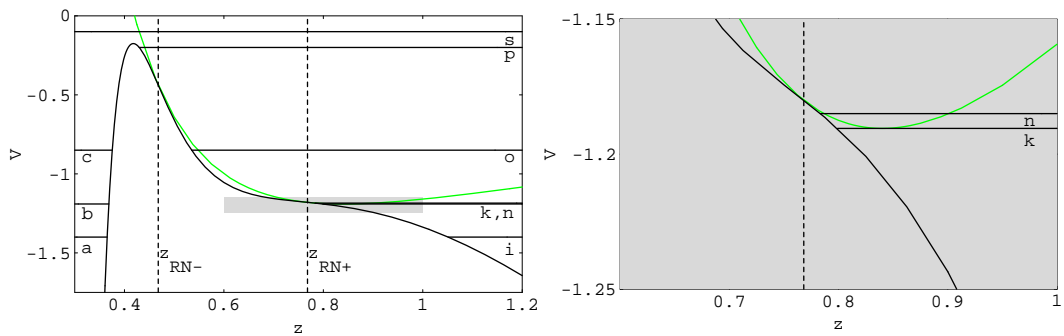


Figure. 14: Reissner-Nordstrom configuration 5.

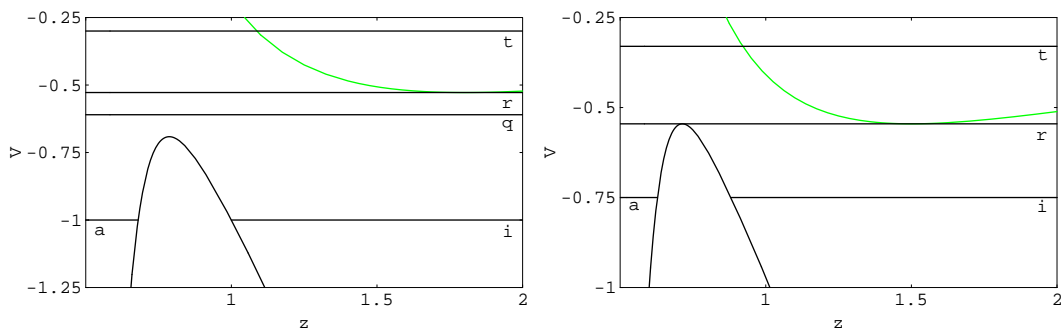


Figure. 15: Reissner-Nordstrom configuration 6 and 7.

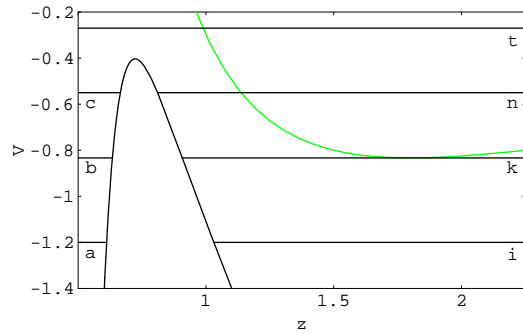


Figure. 16: Reissner-Nordstrom configuration 8.

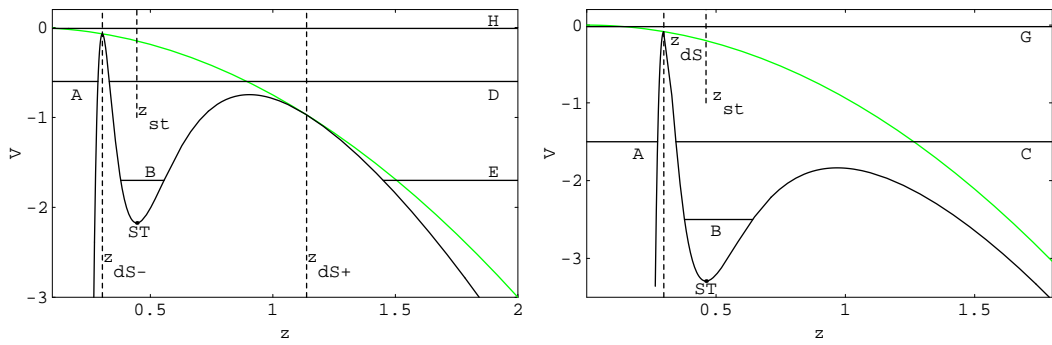


Figure. 17: deSitter configurations I and II.

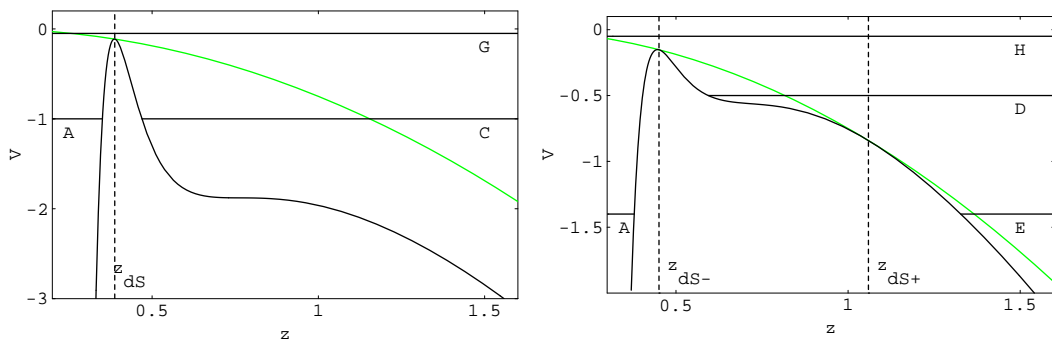


Figure. 18: deSitter configurations III and IV.

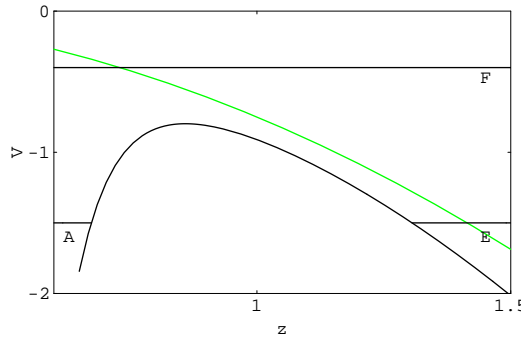


Figure. 19: deSitter configuration V.

References

- [1] J. Bardeen, Proceedings of the GR5 Meeting, Tiflis, U.S.S.R. (1968).
- [2] A. Börde, *Regular Black Holes and Topology Change*, Phys. Rev. D55 (1997) 7615, e-print gr-qc/9612057
- [3] K. Lee, V.P. Nair, E.J. Weinberg, *Black Holes in Magnetic Monopoles*, Phys. Rev. D45 (1992) 2751, e-print hep-th/9112008
- [4] F.A. Bais and R.J. Russell, *Magnetic Monopole Solution of Nonabelian Gauge Theory in Curved Spacetime*, Phys. Rev. D11 (1975) 2692, erratum Phys. Rev. D12 (1975) 3368.
- [5] Y.M. Cho and P.G.O. Freund, *Gravitating 't Hooft Monopoles*, Phys. Rev. D12 (1975) 1588, erratum Phys. Rev. D13 (1976) 531.
- [6] D. Boulware, *Naked Singularities, Thin Shells and the Reissner-Nordstrom Metric*, Phys. Rev. D8 (1973) 2363.
- [7] T. Tachizawa, K. Maeda, T. Torii, *Nonabelian Black Holes and Catastrophe Theory 2: Charged Type*, Phys. Rev. D51 (1995) 4054, e-print gr-qc/9410016
- [8] N. Sakai, *Dynamics of Gravitating Magnetic Monopoles*, Phys. Rev. D54 (1996) 1548, e-print gr-qc/9512045.
- [9] G.L. Alberghi, D. Lowe and M. Trodden, *Charged False Vacuum Bubbles and the AdS/CFT Correspondence*, JHEP 9907:020 (1999), e-print hep-th/9906047.
- [10] G. Arreaga, I. Cho and J. Guven, *Stability of Self-Gravitating Monopoles*, e-print gr-qc/0001078.
- [11] D. Eardley and S.J. Kolitch, *Quantum Decay of Domain Walls in Cosmology: 1. Instanton Approach*, Phys. Rev. D56 (1997) 4651, e-print gr-qc/9706011.
- [12] S. Blau, E. Guendelman, A. Guth, *The Dynamics of False Vacuum Bubbles*, Phys. Rev. D35 (1987) 1747.
- [13] I. Cho, J. Guven, *Modelling the Dynamics of Global Monopoles*, Phys. Rev. D58 (1998) 063502, e-print gr-qc/9801061
- [14] A. Linde and D. Linde, *Topological Defects as Seeds for Eternal Inflation*, Phys. Rev. D50 (2456) 1994, e-print hep-th/9402115.
- [15] A. Vilenkin, *Topological Inflation*, Phys. Rev. Lett. 72 (1994) 3137, e-print hep-th/9402085.
- [16] R. Penrose, *Gravitational Collapse and Spacetime Singularities*, Phys. Rev. Lett. 14 (1965) 57.
- [17] S.W. Hawking and R. Penrose, *The Singularities of Gravitational Collapse and Cosmology*, Proc. Roy. Soc. Lond. A314 (1970) 529.
- [18] T. Cheng and L. Li, *Gauge Theory of Elementary Particle Physics*, Oxford University Press (1984).
- [19] W. Israel, *Singular Hypersurfaces and Thin shells in General Relativity*, Nuovo Cimento 44B (1966) 1; erratum Nuovo Cimento 48B (1967) 463